Proceedings of the ASME 2010 3rd Joint US-European Fluids Engineering Summer Meeting and 8th International Conference on Nanochannels, Microchannels, and Minichannels
FEDSM-ICNMM2010
August 1-5, 2010, Montreal, Canada

FEDSM-ICNMM2010-30287

NUMERICAL SIMULATION OF MONJU PLANT DYNAMICS BY SUPER-COPD USING PREVIOUS STARTUP TESTS DATA

Fumiaki Yamada
Plant Dynamics Analysis Group
FBR Plant Engineering Center
Japan Atomic Energy Agency (JAEA)
1 Shiraki, Tsuruga-shi, Fukui-ken, 919-1279 Japan
Yamada.fumiaki@jaea.go.jp

Hiroaki Ohira
Plant Dynamics Analysis Group
FBR Plant Engineering Center
Japan Atomic Energy Agency (JAEA)
1 Shiraki, Tsuruga-shi, Fukui-ken, 919-1279 Japan
Ohira.hiroaki@jaea.go.jp

ABSTRACT

Flow network models of the upper plenum of reactor vessel and the primary inlet plenum of intermediate heat exchanger (IHX) of MONJU were advanced and each model was validated by the measured data obtained in the previous system start-up tests (SSTs). Then the whole plant dynamics in a plant trip transient of MONJU were simulated by incorporating these flow network models. The natural circulation in the primary and secondary heat transport systems were also validated by these test results. From these validations, we concluded that the plant dynamics model incorporated the advanced models in Super-COPD code could simulate the whole plant dynamics in good accuracy both in the transients and natural circulation conditions and that it was applicable to predict the next SSTs.

1. INTRODUCTION

The plant dynamics analysis code COPD was developed on the basis of mock-up test results for MONJU and validated by the experimental fast reactor JOYO and other mock-up tests for MONJU, but it was not easy to construct proper model of a new plant specification. The flow network models of the main components and control systems were divided into simple calculation modules: These modular programs were renamed as Super-COPD code. Consequently it became possible to construct arbitral flow networks of main components, control systems and whole plants of liquid metal fast breeder reactors (FBRs) (Nakai, et al. (1988) and Tanji, et al. (1986)). However, the thermal-hydraulics in larger regions such as the upper plenum of reactor vessel (RV) could not be predicted well since the structures of the regions in MONJU were modified slightly from the mock-up test facilities. In case of predicting plant dynamics correctly with different sizes and different thermal-hydraulics from the mock-up tests, one dimensional flow network codes such as Super-COPD would be required lots of time and try-and-error procedures to construct proper flow networks.

In RELAP5-3D (The RELAP5-3D Code Development Team (2005)) and CERES (Nishi et al. (2006)) code, main components are calculated by 3 dimensional models and the ducts and other miner components are calculated by one dimensional flow networks. These results are applied as boundary conditions of connected components to realize plant dynamic responses. These approaches are considered to be reasonable. 3 dimensional calculations with reasonable physical models and high resolution meshes can predict the thermal-hydraulics in good accuracy. The plant dynamics predictions are limited in a few cases if such detailed calculations would be applied to the plant dynamics calculations: On the other hand, 3 dimensional calculations become useful for the typical plant dynamics predictions with different sizes and conditions from MONJU, and also makes it possible to construct proper flow networks of the one dimensional codes (Konomura et al. (2009)).

The flow network models of Super-COPD were modified using the above-mentioned experiments and the previous system startup tests (SSTs) of MONJU in order to predict the next SST operations. These results indicated the RV upper plenum and the primary inlet plenum of the intermediate heat exchangers (IHXs) could not predict in good accuracy. In this study, the advanced flow network models of the RV upper plenum and the IHX inlet plenum were validated by the previous SST results. The whole plant dynamics of MONJU

were also predicted using the validated flow networks. The natural circulation experiments both in the primary heat transport system (PHTS) and the secondary heat transport system (SHTS) were also conducted in the previous results. The plant dynamics model with these advanced model was also validated by these natural circulation results. Through these validations, we will show the present plant dynamics model is applicable to the next SSTs and we will also show a reasonable plant dynamics code system for the future FBRs.

2. MODIFICATION OF FLOW NETWORK MODELS

The outline of numerical methods of Super-COPD are reported by Nalkai, et al. (1988) and Tanji, et al. (1986). Hence, the advanced models of the RV upper plenum and the IHX inlet plenum were only described in this section.

2.1 RV upper plenum

2.1.1 Mass and momentum equations

The mass and momentum equations of the upper plenum are shown from Eqs. (1) to (7). The temperature measurements of the upper plenum (the thermocouple tree) and the flow networks are shown in Figs. 1 and 2, respectively. Three momentum equations, which are two levels of flow holes and the upper part of RV, were calculated with the mass conservation equations;

$$C_1 \frac{dW_1}{dt} = \Delta P_1 + \Delta H_1 - f_1 W_1^2, \quad (1)$$

$$C_2 \frac{dW_2}{dt} = \Delta P_2 + \Delta H_2 - f_2 W_2^2, \quad (2)$$

$$C_3 \frac{dW_3}{dt} = \Delta P_3 + \Delta H_3 - f_3 W_3^2, \quad (3)$$

$$W_{in} + W_{pe} = W_1 + W_2 + W_3, \quad (4)$$

$$W_{in} = W_B + W_C, \quad (5)$$

$$W_B + W_{pe} = W_2 + W_4, \quad (6)$$

$$W_5 = W_1 + W_3 = W_C + W_4, \quad (7)$$

where W_i, ΔP_i, C_i, f_i and ΔH_i is the flow rate, the pressure drop, the inertial term, the pressure drop coefficient and the head of the i-th path, respectively. W_{in} is the average flow rate from the outlets of the fuel subassemblies. These momentum equations were discretized implicitly regarding to the pressure drops and the matrices are obtained from Eq. (4). The flow rates of W_1, W_2 and W_3 were calculated by the 2nd order Runge-Kutta method using the calculated pressure drops. These flow paths and calculation methods were not modified in this study. In the previous model, however, W_C was neglected and only averaged inlet flow rate, which was $W_{in} + W_{pe}$, was given as the boundary flow rate. In the present model, the flow rate of W_B was assumed as a constant which was evaluated by the angle of inclination at the bottom of the upper core structure (UCS).

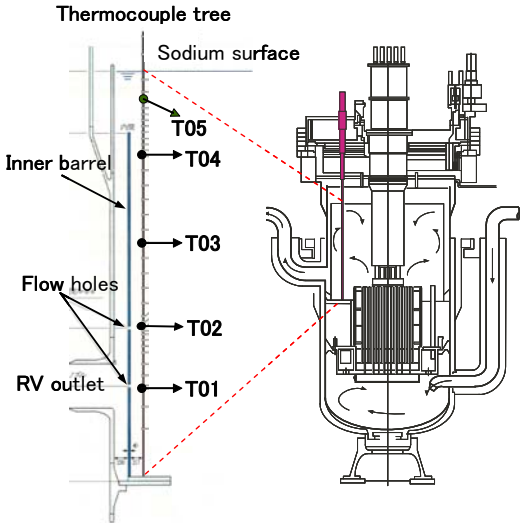

Figure 1. Main measurements on thermocouple tree in RV upper plenum.

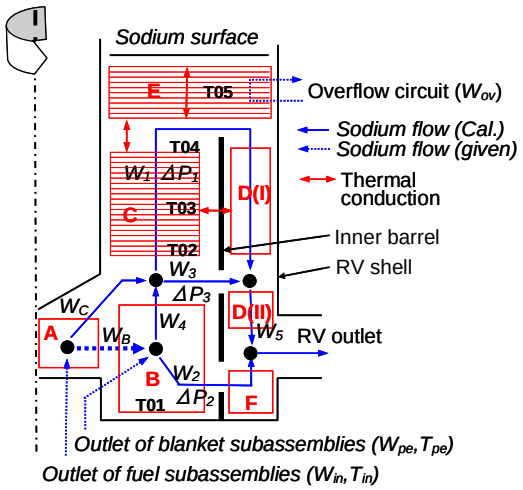

Figure 2. RV upper plenum model of Super-COPD.

2.1.2 Energy equation

The upper plenum was divided into 7 regions, which were A, B, C, D(I), D(II), F and E shown in Fig. 2, and the regions C and E were divided into 20 mesh; the other regions were realized by a complete mixing model. These models are described in Eq. (8);

$$C_p \rho V_X \frac{dT_X}{dt} = C_p \sum_i \left[W_i \left(T_i - T_X \right) \right] + Q , \qquad (8)$$

where C_p, ρ, V_X, T_X are the heat capacity and density of liquid sodium, the volume and temperature of X region. The first term of the right hand side is the amount of heat flowed into the region X from the region i. In Eq. (8), Q is the amount of hest conducted into D(I) from the i-th mesh of the region C through the inner barrel, which are described in Eq. (9);

$$Q = -KS \sum_{i=1}^{n} \left(T_{D(I)} - T_{C,i} \right), \qquad (9)$$

where K and S are the coefficient of overall heat transmission of the inner barrel and the heating surface area, respectively. Eq. (8) is also applied to the region C by replacing T_i and T_X with T_{i-1} and T_i, respectively. Q is also applied by Eq. (10);

$$Q = KS \left(T_{D(I)} - T_{C,i} \right), \qquad (10)$$

The inlet boundary temperature of the region C is averaged by Eq. (11);

$$T_{C,0} = \frac{1}{W_C + W_4} \left(W_4 T_B + W_C T_A \right), \qquad (11)$$

As the flow from the region C to the top region of the plenum E was estimated to be negligible small, the heat transport by the over flow sodium and thermal conduction were modeled in Eq. (8): The flow rate of W_i in Eq. (8) was that of the over flow and Q is applied to Eq. (12);

$$Q = \frac{A_E \lambda}{\Delta z} \left(T_{E,i+1} - 2T_{E,i} + T_{E,i-1} \right), \qquad (12)$$

where λ is thermal conductivity of liquid sodium. All energy equations described in Eq. (8) were also calculated by the 2nd order Runge-Kutta method.

2.2 IHX inlet plenum

The IHX and the close-up of the inlet plenum are shown in Fig. 3. In the previous calculations, the flow network model of the inlet plenum was realized by a complete mixing model without momentum equation, because the IHX of the 50MWSG facility had a simple structure without the rectification shroud and the flow control plate. The calculation results by the simple model were reported to agree well with the experiments. The flow characteristics and the temperature distribution were evaluated by a multi-dimensional code and a 1/2 scaled water experiment. These rectification shroud and flow control plate affected largely to the secondary outlet temperature in these results.

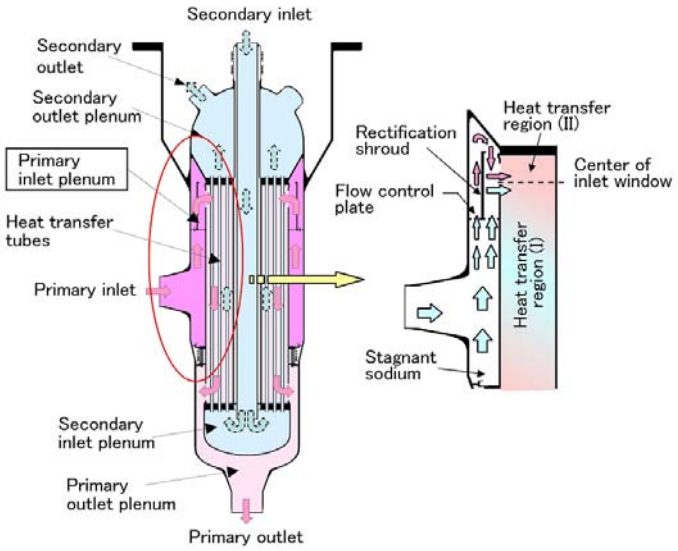

Figure 3. MONJU IHX and close-up of inlet plenum.

Table 1. Flow distributions in inlet plenum

Flow path	*Ratio of Flow Rate (%)*
W_{B1}	$(100-x)\times 0.7$
W_{CA}	$(100-x)\times 0.3$
W_C	$(100-x)\times 0.4$
W_{B2}	$(100-x)\times 0.3$
W_D	$(100-x)\times 0.6$
W_E	$(100-x)\times 0.4$

W_{in}: 100% , W_F: x = 2%

The flow distributions, which are shown in Table 1, and the paths in the inlet plenum, which is shown in Fig. 4, were evaluated and constructed the flow network model by the calculation results and the experiments. The ratios of the flow rate of all the paths shown in Fig. 4 were given in the

calculations, while regions A, C(I) and C(II) shown in Fig. 4 were modeled as complete mixing and regions B(I), B(II), D and E were divided into 20 mesh calculated by the finite difference method. These models were similar to the energy equations of Eq. (8).

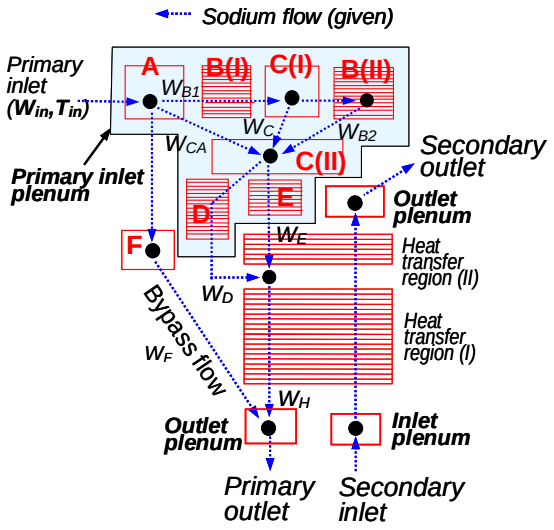

Figure 4. Flow network of IHX inlet plenum.

3. ANALYTICAL CONDITIONS

The analytical conditions are shown in Table 2. The calculations were conducted in 5 cases in this study: The first two cases of Verifs 1 and 2 were conducted to verify the advanced flow network models and the other three cases from Cases 1 to 3 were conducted to validate the whole plant dynamics models. In the RV upper plenum calculation, the flow rate from the fuel subassembly was averaged from the measured flow rate above the outlets, while that from the blanket subassembly was estimated from the difference between the total flow rate and the averaged one.

Table 2. Analytical conditions

Case	*Condition*
Verif 1	*Plant trip from 40% rated power in RV upper plenum*
Verif 2	*Plant trip from 40% rated power in IHX*
Case 1	*Plant trip from 40% rated power in whole plant*
Case 2	*Natural circulation in PHTS by heat release from Primary pumps*
Case 3	*Natural circulation in SHTS by heat release from Primary pumps*

The outlet temperature of fuel subassemblies was also averaged from the measured one, while that of blanket subassemblies was applied the RV inlet temperature. In the IHX calculation, both primary and secondary flow rates were used from the plant trip test from the 40% rated operational power, which was conducted in December 1995. These flow rates were measured by the flowmeters of F1 and F2 in Fig. 5 and the data were shown in Fig. 10. The primary outlet and inlet temperature of IHX were measured at T1 and T2 in Fig. 5 and the data were shown in Fig. 11. The secondary inlet temperature were also applied from the measured ones at T4 and shown in Fig.12.

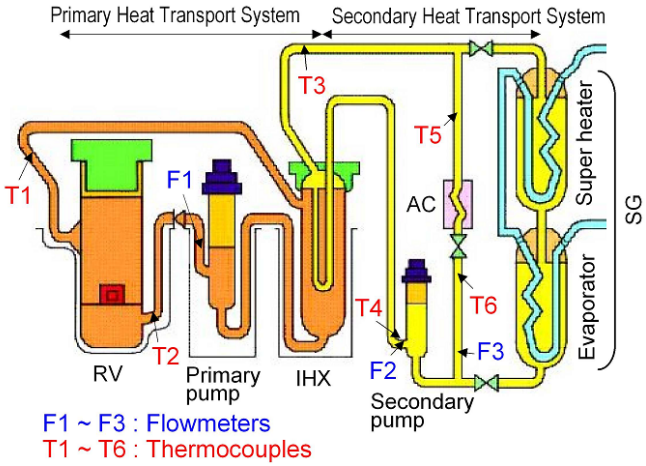

Figure 5. Measurements of MONJU plant.

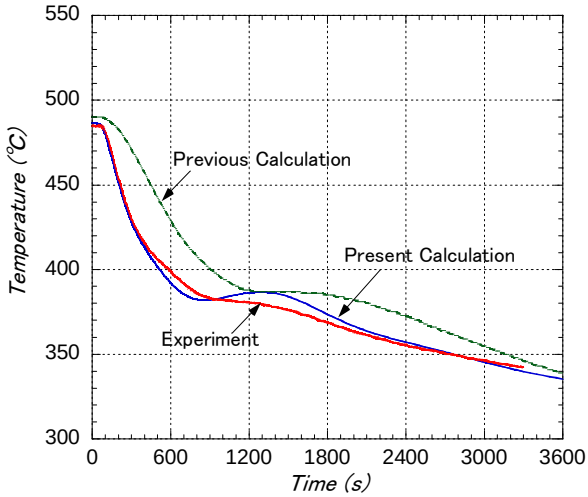

Figure 6. RV outlet temperatures.

4. RESULTS

4.1 RV upper plenum

Outlet temperature of RV measured in the SST and the calculated one by the previous model are shown in Fig. 6. The calculated one is higher than measured one from the reactor scrum (0 s in the figure) to 3600 s; maximum difference is approximately 40 ºC. The colder sodium flows into the upper plenum and mixes with hotter sodium. In this process, some amounts of sodium flow from the two levels of flow holes and the others flow over the inner barrel. The RV outlet temperature is decided by these mixing procedures. Hence, in the previous model, the higher temperature of the calculation is estimated to be caused by the assumption that the averaged outlet temperature flows from all the subassemblies into the B region; consequently, the larger amount of hotter sodium flowed over the inner barrel.

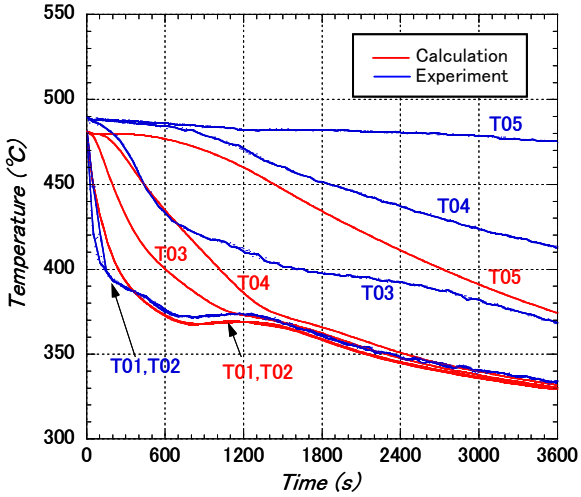

Figure 7. RV upper plenum temperature calculated by previous model.

The typical measured locations of the thermocouples are shown in Fig. 1. Thermocouples of T01 and T02 are installed near the flow holes, while the others (T03, T04, T05) are installed above them. The measured and calculated results at these locations are shown in Fig. 7. The calculated temperatures at T01 and T02 agreed well with the measured ones, since the colder sodium exists under the upper flow holes. On the other hand, the others had large differences between the two kinds of values: The calculated temperature decreased sooner than the measured ones. These differences are estimated the colder sodium rose up inside of the inner barrel sooner than the actual. Therefore, these results indicated the pressure drops at the flow holes and the over flow should be evaluated in detail. The other factor of the differences is estimated the existence of the recirculation flow: The detail examination also indicated the colder sodium from dump tank was flowed into the top region of the upper plenum just after scram till approximately 1200 s. The results by the multi-dimensional thermal-hydraulic analysis also indicated the existence of the stagnant region over the inner barrel. Hence, we modified the flow paths and the pressure drop coefficients at flow holes in the advanced model as shown in Fig. 2. The calculated results by this model (*Verif 1*) are shown in Fig 8 and the RV outlet temperature is also shown in Fig. 6. These temperatures have good agreements with measured ones.

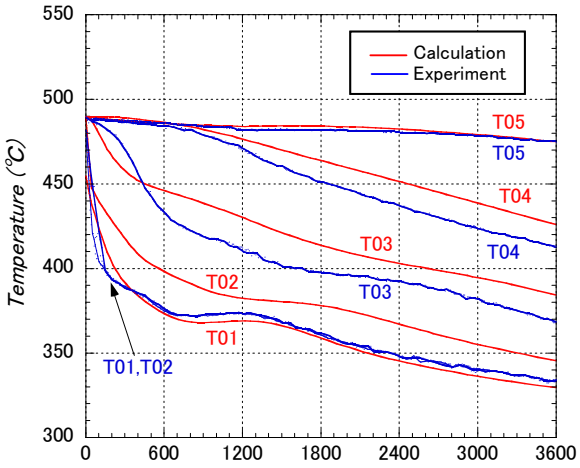

Figure 8. RV upper plenum temperature calculated by advanced model.

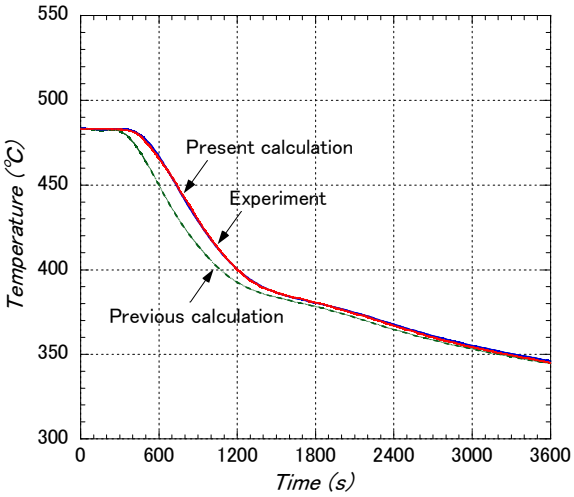

Figure 9. IHX secondary outlet temperature.

4.2 IHX primary inlet plenum

Figure 9 shows the IHX secondary outlet temperatures which were measured in the SST and calculated by the two kinds of models. The temperature calculated by the previous model start to decrease at approximately 300 s and the differences from the measured one are approximately 20ºC until approximately 1200 s. These differences were estimated to be applied the complete mixing model without flow paths in this plenum. However, the results by a multi-dimensional thermal hydraulic calculation and a 1/2 scaled water experiment

indicated this model should be advanced. The results by the advanced model (*Verif 2*) are also plotted in Fig. 9: Agreements with the measured data are fairly good. From these results and the results described in the previous section, it is estimated that a proper multi-dimensional thermal-hydraulic analysis would be required to predict the detailed behavior especially in the different sizes and conditions from MONJU.

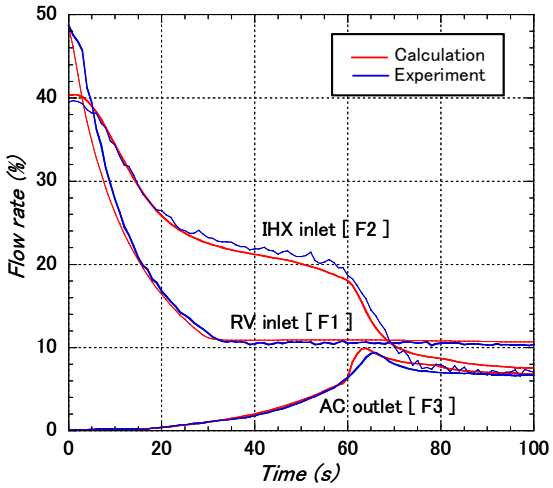

Figure 10. Flow rate of PHTS, SHTS and ACS.

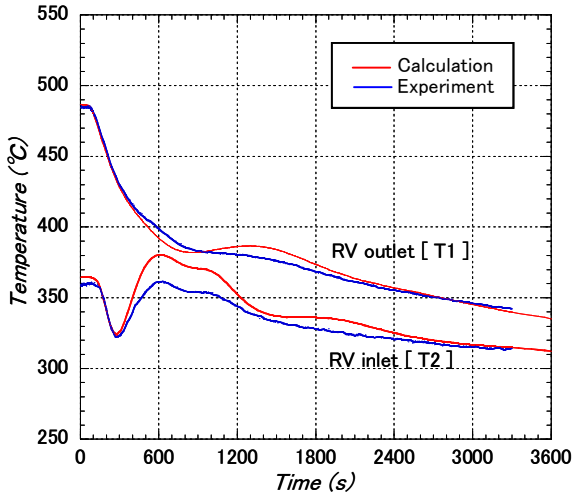

Figure 11. Inlet and outlet temperature of RV.

4.3 Whole plant dynamics

The calculated flow rates of PHTS, SHTS and ACS by the whole plant models in *Case 1*, which were applied the advanced RV and IHX model, are shown in Fig. 10. These flow rates are plotted as the ratios of the 100% rated flow. In this transient, the primary and secondary main pump operations were switched from the flow coast down to the pony motor operations, while the air cooler (AC) operations in the secondary loops were switched from the SG operations. These flow rates agreed well with the measured ones. Therefore, it is estimated that the pump and control models were implemented properly in the present whole plant model. The inlet and outlet temperature of the RV are shown in Fig. 11. The RV outlet sodium temperatures agreed well with the measured ones until 3600 s, which was already shown in the previous section. The calculated inlet sodium temperature was higher than the experiments, which was approximately 20ºC in the maximum value, from approximately 400 to 1300 s.

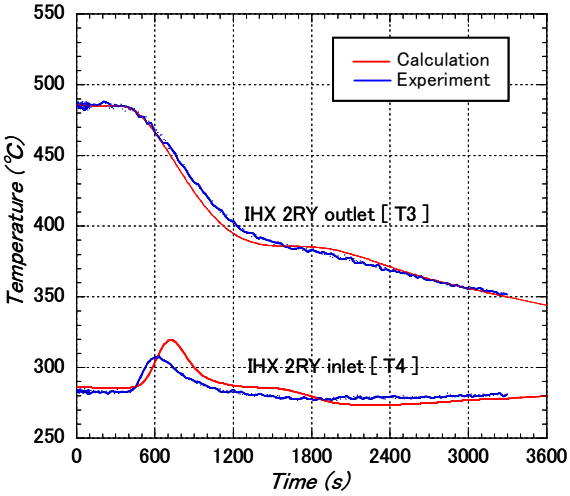

Figure 12. Secondary inlet and outlet temperature of IHX.

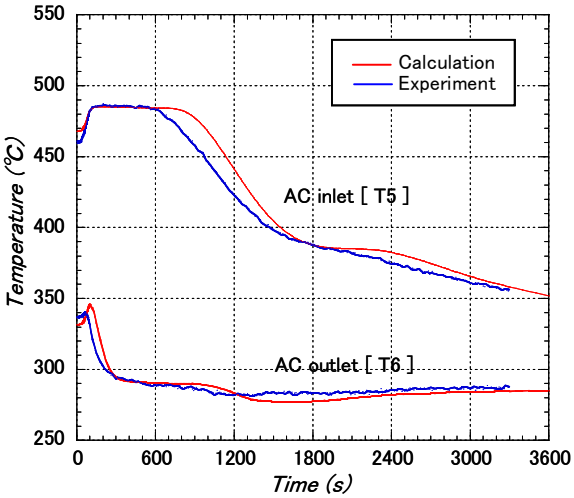

Figure 13. Inlet and outlet temperature of AC.

The inlet and outlet temperature of the air cooler (AC) in ACS are shown in Fig. 13. The peak outlet temperature appeared approximately 50 s later than the measured one and the higher temperature keeps until 300 s. These differences affected the peak temperature difference of the secondary inlet

temperature of IHX as shown in Fig. 12 and finally affect the second peak temperature of the RV inlet temperature. On the other hand, the AC inlet temperature started to decrease approximately 200 s later than the experiments. Since the maximum temperature agreed well with each other, these differences were estimated to be caused by the delay of operation timing of the AC vane and damper throttling. These differences would not affect largely and would be easily corrected in the future. The most important modification in the present model is considered to be the primary outlet plenum of IHX with the proper multi-dimensional thermal-hydraulic analysis.

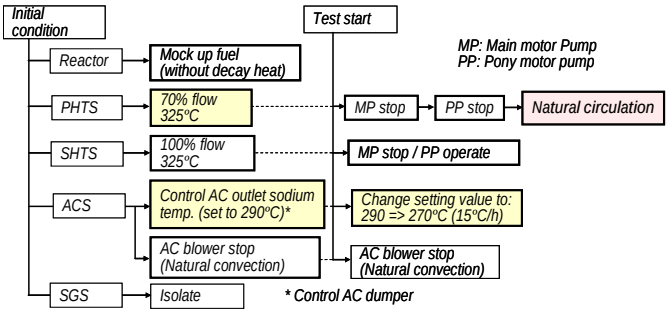

Figure 14(a). Sequence of natural circulation in PHTS (Case 2).

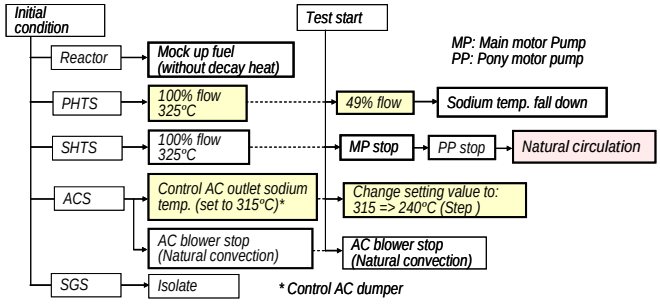

Figure 14(b). Sequence of natural circulation in SHTS (Case 3).

4.4 Natural circulation

The whole plant trip transient was calculated in good accuracy by introducing the advanced models of RV upper plenum and IHX primary inlet plenum. However, this model would not be applicable to natural convection since the temperature and the flow rate of the heat transport system would change slowly compared with the plant trip transients. In this section, the upper plenum model of RV was modified to a simple model in order to apply to the slow transients. In the previous SSTs, two kinds of natural circulation tests were conducted; one is for the PHTS and another is for the SHTS. Both tests simulated the core decay heat by the heat released from the primary pumps. The divided regions of A, B, C and E of the advanced RV model were unified as one region with complete mixing model and those of D(I), D(II), F were also unified as another region with complete mixing model. The heat transfer coefficients of IHX and AC were also modified to the experimental correlations evaluated from the 50MWSG facility and JOYO (Mochizuki and Takano (2009)). The sequences of the primary and the secondary natural circulation tests are shown in Figs. 14(a) and 14(b) (*Cases 2 and 3*), respectively.

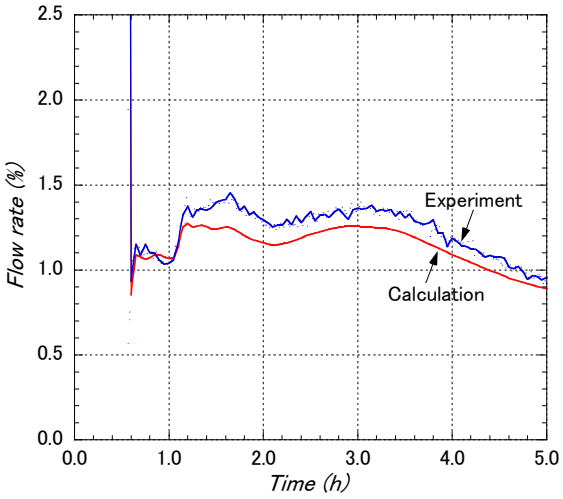

Figure 15. Flow rate of PHTS in primary natural circulation test.

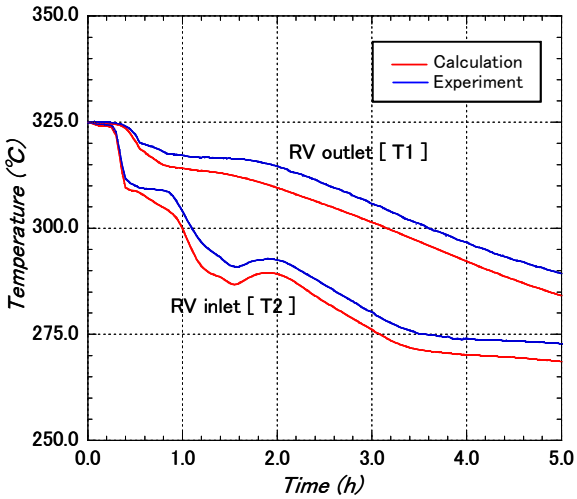

Figure 16. RV inlet and outlet temperature in primary natural circulation test.

The flow rate of the PHTS and the RV inlet and outlet temperature in Case 2 are shown in Figs. 15 and 16,

respectively. Natural circulation is produced after the pony motor operation was stopped in approximately 30 minutes and the measured flow rate was in the range from 1.0 to 1.5% of the rated flow. The calculated flow rate showed the similar trends but had 0.1 to 0.2% lower flow rate, which was approximately 10% lower compared with the experiments. The RV inlet and outlet temperature also showed the similar trends but had approximately 5ºC lower than the experiments. In this natural circulation, only heat sink existed in IHX, so the buoyancy force was produced from the temperature difference between the inlet and outlet of IHX. From these results, it is estimated that the buoyancy force was properly modeled in Super-COPD and the RV upper plenum model was also proper.

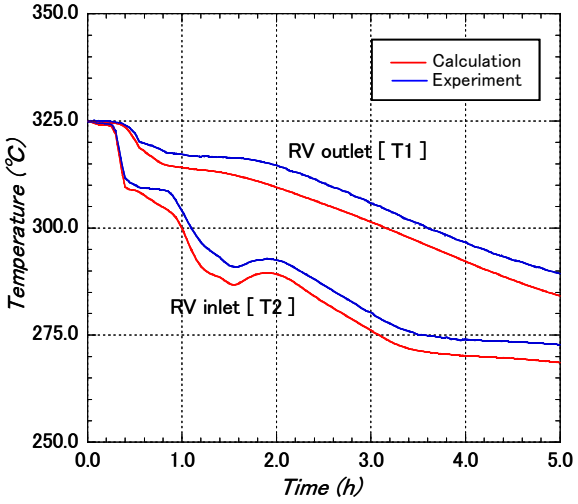

Figure 17. Flow rate of SHTS in secondary natural circulation test.

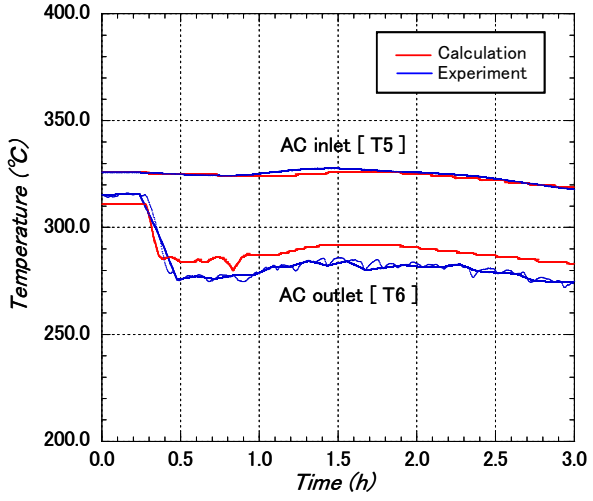

Figure 18. AC inlet and outlet temperature in secondary natural circulation test.

The flow rate of the SHTS and the AC inlet and outlet temperature in Case 3 are shown in Figs. 17 and 18, respectively. The calculated flow rate agreed well with the experiments after the natural circulation was produced. The calculated AC inlet temperature also agreed with the experiment, but the outlet temperatures were approximately 5ºC lower than the experiments. The heat sink and source are AC and IHX, respectively in these conditions. Therefore, in this calculation, the buoyancy force was also properly modeled in Super-COPD. From these two kinds of results, the slow transient would be predicted by the simple RV upper plenum model when the buoyancy force is properly modeled.

CONCLUSIONS

The advanced flow network models of the RV upper plenum and the IHX inlet plenum of MONJU were validated by the previous SST results. The whole plant dynamics of MONJU were also predicted using the validated flow networks. The natural circulation experiments both in the PHTS and the SHTS were conducted applying the previous SST conditions. The whole plant dynamics model with the advanced model was also validated by these test results. From these validations, the present plant dynamics model of Super-COPD could simulate the whole plant dynamics in good accuracy, which was applicable to the next SSTs. We will continue to verify and validate Super-COPD code by the next SST results.

REFERENCES

Konomura, M., et al., “Future R&D programs using MONJU,” International Conference on Fast Reactors and Related Fuel Cycles (FR09), Paper No. IAEA-CN-176-01-11,December (2009).

Mochizuki, H. and Takano, M., “Heat transfer in heat exchangers of sodium cooled fast reactor systems,” Nuclear Engineering and Design, Vol. 239, 295-307 (2009).

Nakai, S., et al., “Development of Module Integrated Plant Dynamics Analysis Code -Development of Super-COPD Code-,” PNC Technical review No. 68-3 (1988) (in Japanese).

Nishi, Y., et al., “Verification of the plant dynamics analysis code CERES using the results of the plant trip test of the prototype fast breeder reactor MONJU,” Proc. of the 14th International Conference on Nuclear Engineering, CD-ROM, No. ICONE14-89386, July (2006).

Tanji, M., et al., “Development and Verification of a Thermo-Hydraulic Simulation Code for System Transient in “Monju” (COPD code),” MHI Technical review Vol. 23, No. 6 (1986) (in Japanese).

The TELAP5-3D Code Development Team, “RELAP5-3D Code Manual, Volume I: Code Structure, System Models and Solution Methods,” INEEL-EXT-98-00834, Revision 2.4 (2005), http://www.inl.gov/relap5/r5manuals.htm.